Satellite passive microwaves reveal climate-induced carbon losses in African drylands, 2010-2016

Martin Brandt[1], Jean-Pierre Wigneron[2], Jerome Chave[3], Torbern Tagesson[1], Josep Penuelas[4,5], Philippe Ciais[6], Kjeld Rasmussen[1], Feng Tian[1], Cheikh Mbow[7], Amen Al-Yaari[2], Nemesio Rodriguez-Fernandez[2], Guy Schurgers[1], Wenmin Zhang[1], Jinfeng Chang[6], Yann Kerr[9], Aleixandre Verger[4,5], Compton Tucker[10], Arnaud Mialon[9], Laura Vang Rasmussen[1], Lei Fan[2], Rasmus Fensholt[1]

[1] Department of Geosciences and Natural Resource Management, University of Copenhagen, 1350 Copenhagen, Denmark.

[2] ISPA, INRA Bordeaux, France

[3] Laboratoire Evolution and Diversité Biologique, Bâtiment 4R3 Université Paul Sabatier, 118 route de Narbonne, 31062 Toulouse cedex 4, France

[4] CSIC, Global Ecology Unit CREAF-CSIC-UAB, Bellaterra, 08193 Catalonia, Spain

[5] CREAF, Cerdanyola del Vallès, 08193 Catalonia, Spain

[6] Laboratoire des Sciences du Climat et de l'Environnement, CEA-CNRS-UVSQ, CE Orme des Merisiers, 91191 Gif sur Yvette, France

[7] START International Inc., 2000 Florida Ave NW, Washington, DC 20009, USA.

[8]International Institute for Earth System Sciences, Nanjing University, 210023 Nanjing, China.

[9] CESBIO, Université de Toulouse, CNES/CNRS/IRD/UPS, Toulouse, France

[10] NASA Goddard Space Flight Center, Mail Code 610.9, Greenbelt, MD 20771, USA

Introductory paragraph

The African continent is facing one of the driest periods in the past three decades and continuing deforestation. These disturbances threaten vegetation carbon (C) stocks and highlight the need for improved capabilities of monitoring large-scale aboveground carbon stock dynamics. Here we used a new satellite data set based on vegetation optical depth derived from low frequency passive microwaves (L-VOD) to quantify annual aboveground woody carbon changes in sub-Saharan Africa between 2010 and 2016. Gross gains in carbon stocks (+1.74 Pg C y^{-1}) were slightly overbalanced by gross losses (-1.84 Pg C y^{-1}) of which ~40% (-0.7 Pg C y^{-1}) occurred in drylands (53% of the land area). The overall net change in drylands was -0.07 Pg C y^{-1} associated with drying trends, and a net change of -0.03 Pg C y^{-1} was observed in humid areas. These trends reflect a high inter-annual variability with very wet years (2011 and 2013; net changes +0.33 and +1.13 Pg C) and a very dry year (2015; net change -1.1 Pg C) associated with carbon gains and losses respectively. This study demonstrates, first, the applicability of L-VOD to monitor the dynamics of carbon loss and gain due to climate variations, and second, the importance of the highly dynamic and vulnerable carbon pool of dryland savannahs for the global carbon balance, despite the relatively low carbon stock per unit area.

Introduction

The forests and savannahs of Africa have attracted particular attention because both climate change and land-use pressure have large impacts on the carbon stocks of woody vegetation, with immediate consequences for the global carbon balance[1-4]. Whereas deforestation is a well-known threat to rainforests[2,5-8], savannahs occur in areas of climatic extremes and the mostly sparse vegetation is very sensitive to dry years[9]. However, the net balance of carbon stocks in the savannah vegetation, changes in plant growth rates (negatively impacted by humans and dry periods but positively affected by elevated CO_2[1]) and altered mortality of the woody vegetation are currently unknown[10,11]. We also do not know if semi-arid Africa, which was identified as an important carbon sink with a peak in the extremely wet year of 2011[12], has become a carbon source following the recent extreme El Nino in

2015-2016[13]. Recent work showed that the number of trees in global drylands has been greatly underestimated[14]: a carbon stock neglected in global assessments[15]. Knowledge of the amount, distribution, and turnover of carbon in African vegetation is crucial for understanding the effects of human pressure and climate change[16], but the shortcomings of optical and radar satellite products and the lack of systematic field inventories have led to considerable uncertainty in documenting patterns of carbon stocks, and their long-term change over the African continent[3,4]. Static carbon maps have been developed based on field plots and satellite data using LIDAR, visible/infrared reflectivities and radar backscattering. These maps constitute the best benchmarks to date for carbon stored in the live woody vegetation[17-21]. The application of different techniques, however, complicates the direct comparison of these maps, and results differ in magnitude and spatial patterns[20]. Importantly, also the temporal dynamics of carbon stocks cannot be derived from the above benchmark maps, impeding timely, repeated, and reliable carbon assessments[22].

In contrast, the vegetation optical depth (VOD) derived from high frequency (>5 GHz) passive microwave-based satellite systems has been used to monitor changes in vegetation carbon[23,24]. Although the coarse spatial resolution of passive microwaves (43 km gridded at 25 km) has limited their application for detecting the spatial extent of deforestation, this technology is an attractive alternative to other remote sensing systems because microwaves at frequencies lower than 15 GHz are almost insensitive to atmospheric and cloud effects. However, high frequency VOD saturates over forested areas and is generally not considered as an accurate tool for carbon monitoring[5,7]. The Soil Moisture and Ocean Salinity (SMOS) mission launched in 2009 was the first passive microwave-based satellite system operating at L-band (1.4 GHz) frequency[25]. These low frequencies allow the satellite to sense deeper within the canopy layer with less influence by the green non-woody plant components. The VOD derived from SMOS, henceforth L-VOD, is thus less sensitive to saturation effects[26], marking an important step forward in the monitoring of carbon as a natural resource. In this study, we apply for the first time L-VOD to quantify the inter-annual dynamics of aboveground carbon stocks for the

period 2010-2016. This study does not attempt at improving current aboveground carbon stock maps nor at a comparison with state-of-the-art data and maps on carbon stocks[24,19,21]. Based on calibrated relationships between L-VOD and an existing benchmark map we present and analyse temporal patterns of gains and losses in different humidity zones of sub-Saharan Africa in response to recent dry years.

RESULTS

Estimating Africa's carbon stocks with passive microwaves

L-VOD averaged for 2010-2016 was linearly correlated with a benchmark map on aboveground live biomass carbon (hereafter the term carbon stocks is used) over Africa[20] (Fig. 1a). Although the benchmark map contains bias and uncertainties (Supplementary Fig. 1, Supplementary Table 1), the comparison clearly demonstrates the strong relationship between L-VOD and carbon stocks. The reference map[20] was thus used as a training set to convert L-VOD to carbon per unit area (Mg C ha^{-1}). The L-VOD carbon density map was strongly and linearly correlated with the reference map (cross validated r^2=0.92 and *RMSE*=12 Mg C ha^{-1}, p<0.01, n=26199) (Supplementary Figs 1,2). Baccini et al.[20] reported the total C stocks of Africa to be 64.5 Pg C (±13 at the 95% confidence level (CL)), which was reproduced (Fig. 1b) using L-VOD predicting a C stock of 64.0 Pg C (±10 at the 95% CL, estimated by 10-fold cross validated *RMSE*). In contrast to L-VOD, high-frequency X-band VOD[24] from AMSR-2 saturated for values >100 Mg C ha^{-1} (Fig. 1b) and optical satellite data for values >50 Mg C ha^{-1} (Supplementary Fig. 2).

We stratified the L-VOD time series analysis of African vegetation into (1) drylands versus humid areas, as defined by the ratio between annual precipitation and potential evapotranspiration[14], and (2) four merged land cover classes[27] (Supplementary Table 1). The ability of L-VOD to predict C stocks was similarly strong for both drylands at 10.5±2.9 Pg C (r^2=0.74, p<0.01, *RMSE*=2.4 Mg C ha^{-1}, n=13418) and for humid areas at 53.1±7.9 Pg C (r^2=0.92, p<0.01, *RMSE*=7.5 Mg C ha, n=12781).

The spatial distribution of carbon stocks at continental scales was relatively even among the land cover classes, with open trees/shrubs (including agricultural lands) comprising almost half the carbon stocks of rainforests (Supplementary Table 1). Mean carbon density was correlated with mean soil moisture and mean annual rainfall with changing classes of land cover along the rainfall gradients (Fig. 1c,d). The correlation between carbon density and rainfall disappears at around 1600 mm rainfall, and carbon density was markedly higher for rainforests than for the remaining classes (Fig. 1d).

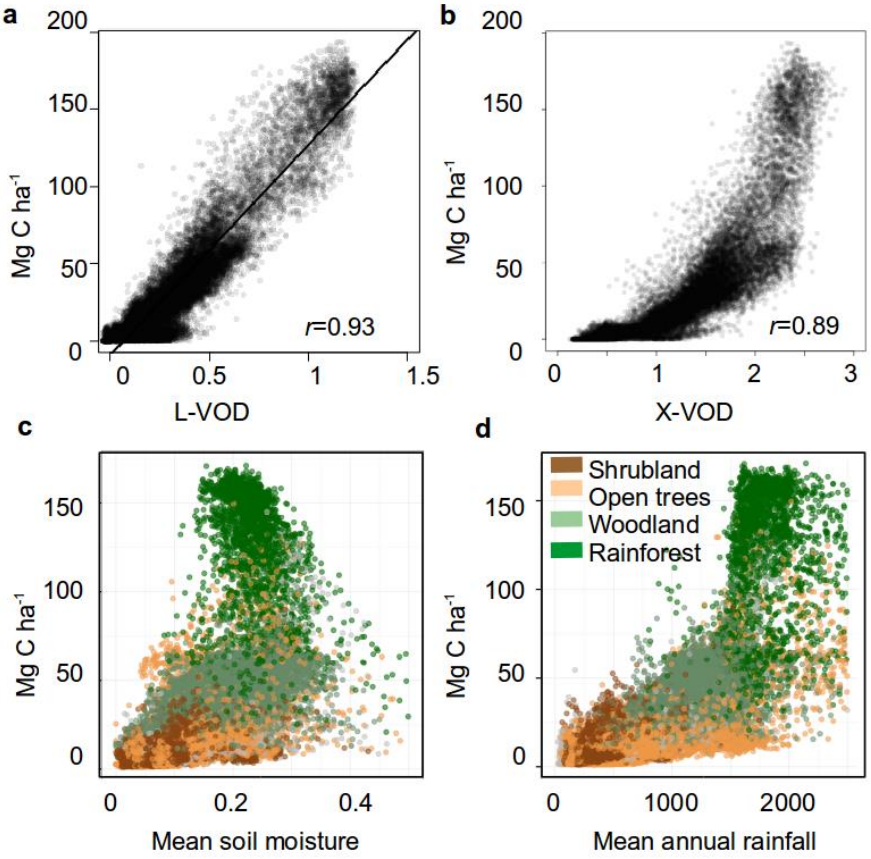

Figure 1: Relationships between carbon density in biomass and VOD in sub-Saharan Africa. a, *Regression between biomass carbon density from Baccini et al.[20] (obtained from GLAS space-borne data and forest inventories 2007/2008) and average low frequency L-VOD (2010-2016) from this study, showing no saturation in the relationship.* ***b,*** *Same regression with high frequency X-band VOD from AMSR-2 (average 2012-2015); This relationship saturates at biomass values > 100 Mg C ha^{-1}.* ***c,*** *Relationship between L-VOD estimated carbon density (mean 2010-2016) and SMOS-IC surface soil moisture (mean 2010-2016) and with* ***d,*** *mean annual rainfall (CHIRPS) for 2010-2016 (colours*

attribute a land-cover class to each pixel of 25 x 25 km).

Africa's carbon stocks are highly dynamic

To compute annual changes in C stocks, the coefficients derived from the relationship between Baccini's aboveground biomass carbon map[20] and mean L-VOD (Fig. 1a) were applied for each yearly median L-VOD map separately. This space-for-time substitution was applied because no inventory data at such a fine temporal resolution were available. Significant trends in carbon were found using per-pixel linear trends in annual carbon density for 2010-2016 (p<0.05, 7 years) (Fig. 2a). Carbon net changes (increases and decreases) were computed by comparing the difference in C stocks between the years 2010 and 2016 (Supplementary Table 1). Gross losses and gains were calculated by cumulating positive (respectively, negative) changes between all the consecutive years from 2010 to 2016 (Fig. 2b-f). Gross changes are larger than net changes as losses and recovery occur in the same pixel/region over the study period. The balance between gross gain and gross loss equals the net changes and is shown in Fig. 2b.

Over the study period, net changes in carbon were relatively balanced in most latitudinal bands (Fig. 2c). Across sub-Saharan Africa, gross gains (+1.74 Pg C y^{-1}) were offset by gross losses (-1.84 Pg C y^{-1}) with an overall negative net carbon budget for Africa (-0.1 Pg C y^{-1}). The majority of the net losses occurred in drylands (-0.07 Pg C y^{-1}) and humid areas experienced a smaller carbon loss (-0.03 Pg C y^{-1}). Notably, a gross carbon loss of -0.7 Pg C y^{-1} occurred in drylands and is partly compensated by a gross gain of +0.63 Pg C y^{-1}. This gross loss per year represents ~5% of the dryland total carbon stocks in Africa (10.3±3.2 Pg C in 2010) (Fig 2f). By contrast, yearly gross losses from humid areas represent ~2% (-1.13 Pg C y^{-1}) of the total stock (54.9±8.1 Pg C in 2010), with noticeable areas in the Democratic Republic of Congo, Ethiopia, Uganda, Ivory Coast, Ghana and Nigeria (Fig. 2b,d). Gross gains in humid areas were +1.10 Pg C y^{-1} mainly located around the central African forest of the Congo basin (Fig. 2b,c,e,f). The magnitude of gross fluxes being much larger than net fluxes illustrates the highly dynamic variations of carbon stocks during the study period.

Areal and net changes in carbon stocks were close to zero when averaged per land cover class at continental scale (Fig. 2h) except in the open trees/shrubs class with gross gains being 0.09 Pg C y^{-1} below gross losses (Supplementary Fig. 5, Table 1). Using Senegal as a case study site, the observed L-VOD decrease was related with a mass dying of shrubs (2013-2015) caused by a prolonged dry period which was documented by very high spatial resolution satellite and field data from 2015, see ref [28] for further documentation of this event (Fig. 3, Supplementary Fig. 6). Stocks of woodlands considerably increased north ~10°S but decreased further south. Gross losses in rainforests were -0.3 Pg C y^{-1}, presumably caused by deforestation (Fig. 2b-d). Gross gains (-0.29 Pg C y^{-1}) almost compensated C losses in rainforests. Using a simple bookkeeping model, Houghton et al.[29] reported an annual carbon loss from deforestation of -0.4 Pg C y^{-1} in Africa, which is comparable to our observed values for rainforests (-0.3 Pg C y^{-1}), although below-ground biomass carbon changes and delayed soil carbon emissions after deforestation, which are part of the bookkeeping model[29], are not included in the L-VOD based carbon estimates.

For individual years, the largest net losses (-1.1 Pg C for all Africa, -0.39 for drylands and -0.73 Pg C for humid areas) were for found in 2015 (Fig. 2g), which is a comparable numbers as the net carbon fluxes measured by the Orbiting Carbon Observatory-2 for tropical Africa (-0.8 Pg C) during the severe El Niño[30]. Overall positive net changes were observed in 2011 (+0.33 Pg C) and 2013 (+1.12 Pg C). Interestingly, net changes in 2014 were positive in drylands.(+0.16 Pg C) but negative in humid areas (-0.28 Pg C). Contrastingly, the year 2016 was a considerable C source in drylands (-0.42 Pg C) but a sink for humid areas (+0.2 Pg C).

We applied two ecosystem models to test the performance of state-of-the-art methods commonly used to assess large-scale temporal C dynamics. The spatial patterns of carbon stored in woody vegetation simulated by LPJ-GUESS (r=0.85, p<0.01) and ORCHIDEE-MICT (r=0.87, p<0.01) agreed reasonably well with L-VOD carbon estimations (Fig. 2i; Supplementary Fig. 2). Drylands, however, showed a share of the total pool of African carbon stocks of 17% in L-VOD but only 6% in LPJ-GUESS and 8% in ORCHIDEE-MICT, possibly because models describe vegetation as either grass

or tree plant functional types but do not incorporate mixed types occurring in savannahs.

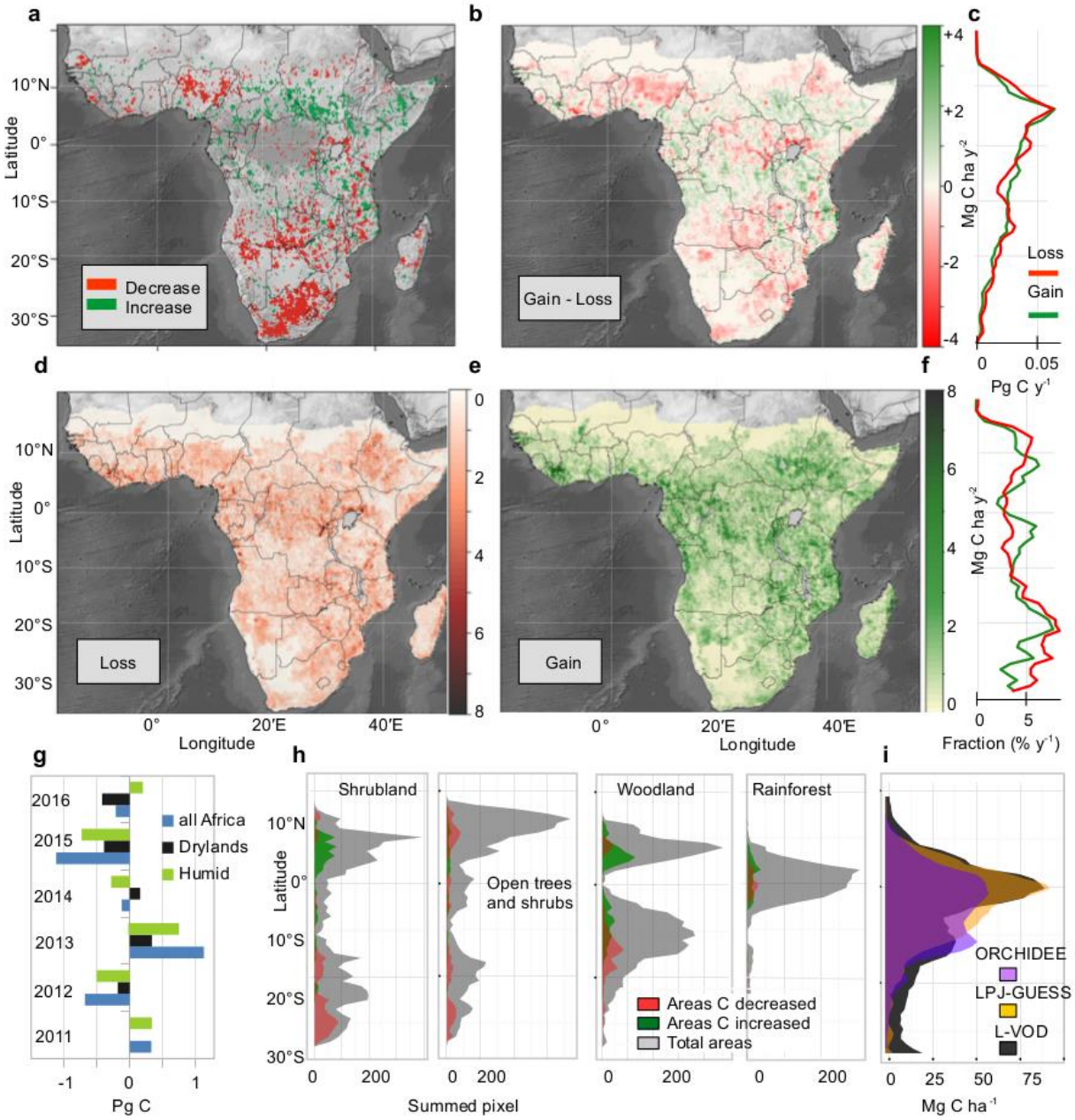

Figure 2: Changes in carbon stocks for 2010-2016. a, *Pixels of significant ($p<0.05$) positive (green) and negative (red) changes (linear trend; $p<0.05$) in aboveground carbon density based on L-VOD for the 2010-2016 period.* ***b,*** *Net changes in C density between 2010 and 2016.* ***c,*** *latitudinal sums of gross losses and gains.* ***d,*** *Cumulative gross losses (time integral of losses) and* ***e,*** *cumulative gross gains in C density.* ***f,*** *Fractional gross losses and gains per year in the L-VOD data.* ***g,*** *Net carbon changes for individual years.* ***h,*** *Areas affected by significant ($p<0.05$) positive (green) and negative*

(red) changes in carbon density for L-VOD 2010-2016 summed per latitude band. ***i,*** *Latitudinal averages of L-VOD carbon density (dark grey) compared to LPJ-GUESS (orange) and ORCHIDEE-MICT (purple) simulated values of above ground biomass carbon.*

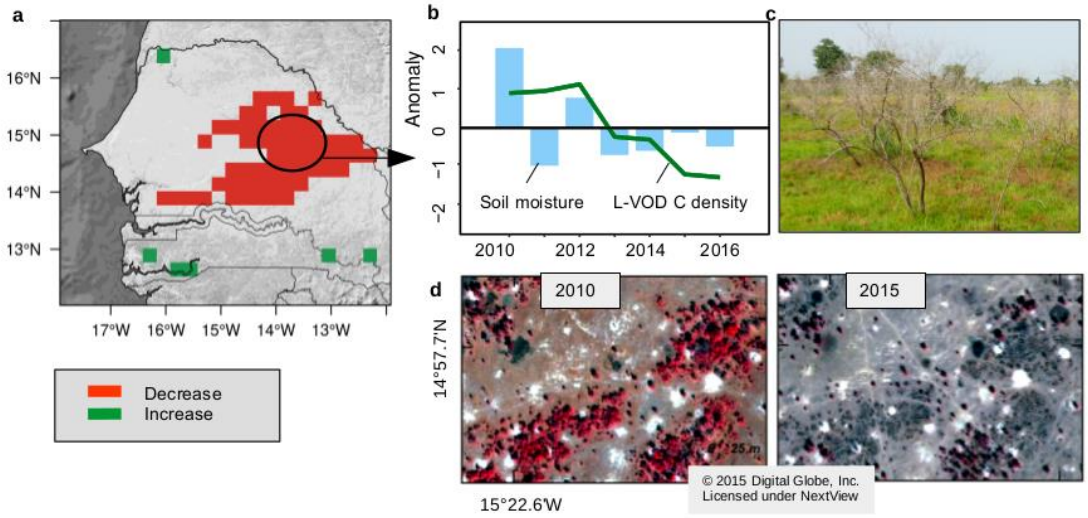

Figure 3: Shrub die off in Senegal. a, *Pixels of significant changes (linear trend; $p<0.05$) in L-VOD carbon density (2010-2016).* ***b,*** *L-VOD carbon density (average of pixels in the circle) decreased rapidly after 2013, reflecting widespread mortality of Guiera senegalensis shrubs between 2013 and 2015 due to a prolonged dry period. This event was documented by* ***c,*** *field photos (2015) and* ***d,*** *very high spatial resolution satellite imagery (from the WorldView-2 and QuickBird-2 satellites; Supplementary Fig. 6)*[28].

Recent dry periods have reduced carbon stocks in dryland areas

Soil moisture[31] showed similar latitudinal patterns as L-VOD carbon density and explained a large fraction of the observed dynamics in carbon stocks between 2010 and 2016 (Fig. 4a,b). Although the fire frequency increased in 2016, fewer fires occurred in areas of major L-VOD decreases (Fig. 4c). These recent decreases in L-VOD estimated carbon stocks were most dramatic in southern Africa, which was approximately reproduced by the ecosystem models (Fig. 4d,e). Moreover, rainfall data[32] and vegetation greenness indicated abnormally dry conditions in most parts of Africa in recent years, particularly during the severe El Niño episode of 2015/2016 (Fig. 4f,g), indicating that dry years have

196 caused the changes in L-VOD, rather than impacts from human disturbance and fires. Prior to 2010,
197 conditions were stable and extraordinarily positive anomalies in carbon density and soil moisture
198 were recorded for 2011 (Fig. 4a,b), confirming previous studies based on ecosystem models and
199 greenness satellite data[12]. After 2011, carbon stocks estimated by L-VOD and simulated by ecosystem
200 models decreased considerably (Fig. 4b,d,e) and southern Africa turned from being a carbon sink into
201 a source, with considerable carbon losses in 2015/2016. Simulations by ecosystem models suggested
202 that the negative trend in dryland carbon stocks persisted over the 1982-2015 period, beyond the
203 SMOS observation era (Fig. 4h-j). Simulated increases in humid areas around 5°N-10°S were less
204 strong in L-VOD (Fig. 4e), but observed decreases around 0° were not shown in the climate driven
205 ecosystem models, suggesting deforestation.
206 Overall, most of the detected decreases in carbon stocks were related with abnormally low soil mois-
207 ture (Fig. 5a). Note however that neither rainfall nor soil moisture can explain the large-scale in-
208 creases of carbon for ~5ºN that may either reflect non-symmetrical net primary productivity responses
209 to wet years (positive convexity), improved forest management or a decrease in wood fuel gathering
210 in regions affected by conflicts and migration to urban areas (such as South Sudan, Central African
211 Republic). At country scale, carbon stocks were found to increase in Sudan, the Central African Re-
212 public, Cameroon, Gabon, Congo, Somalia, and Tanzania (Fig. 5b), in spite of mostly dry conditions
213 and significant FAO reported deforestation in these countries[33]. Carbon stocks decreased considerably
214 in Ghana, Ivoy Coast, Nigeria, Uganda and Zambia, which may partly be caused by deforestation.
215 Despite their lower woody covers compared to forested areas, large losses of carbon were found in
216 South Africa, and are related with dry years.
217 The sensitivity of inter-annual variability in carbon density to dry years was assessed by a Spearman
218 rank correlation between carbon density and soil moisture (Fig. 5c; Supplementary Fig. 7). This
219 showed that country level carbon stocks were less sensitive to dry years in countries of humid regions
220 whereas stocks were most sensitive in countries of drylands.
221

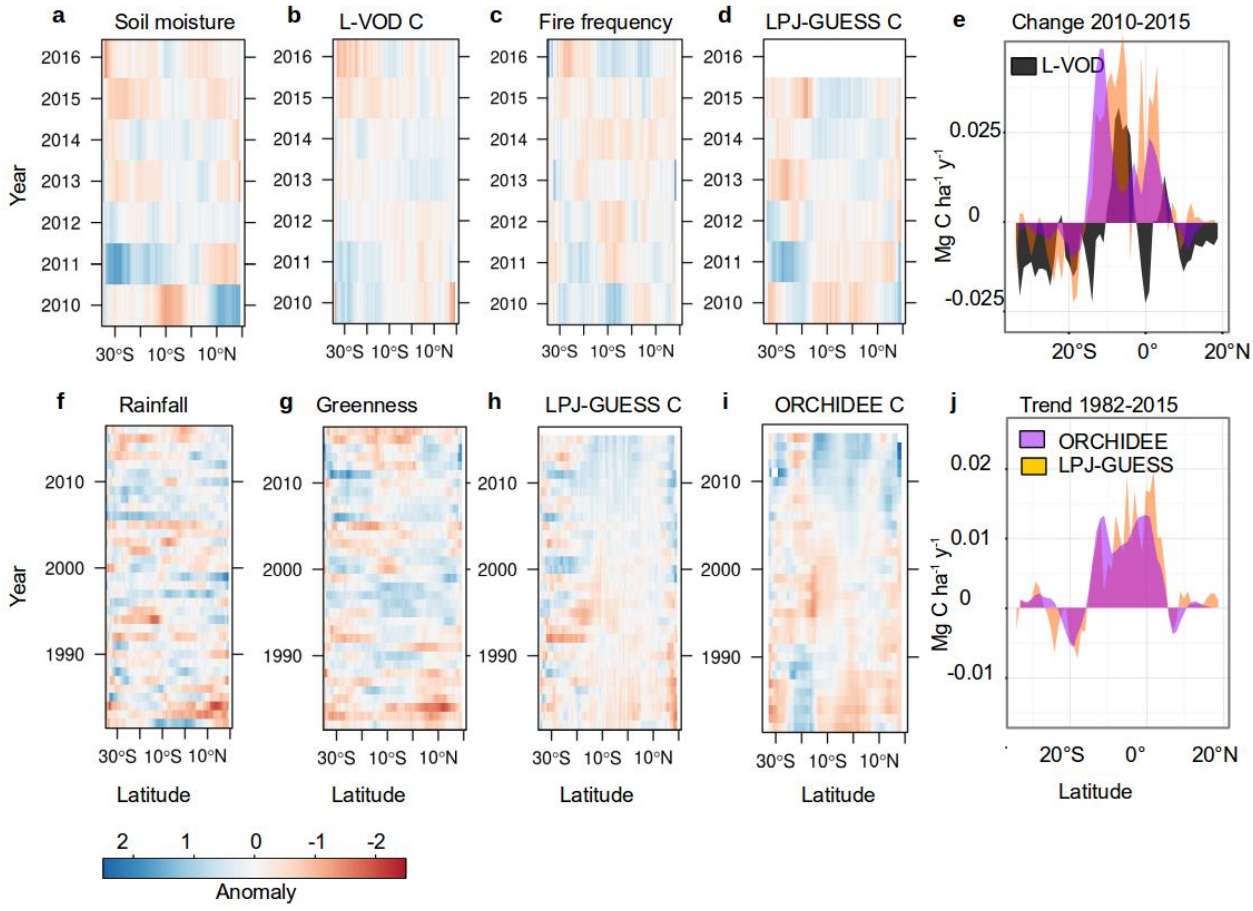

Figure 4: Hovmöller diagrams showing anomalies (z-score) for Africa for each year and latitude. ***a,*** *Anomalies for 2010-2016 of SMOS soil moisture,* ***b,*** *L-VOD carbon density,* ***c,*** *MOD14CMH fire frequency* ***d,*** *LPJ-GUESS simulated aboveground woody carbon density. Model results for the year 2016 could not be displayed because harmonized gridded climate forcing data were not available to drive these models at the time of this analysis.* ***e,*** *Change of aboveground carbon density simulated by the ecosystem models and observed in the L-VOD product between 2010 and 2015.* ***f,*** *Anomalies for 1982-2016 of the number of rainy days (>1 mm),* ***g,*** *vegetation greenness (annually summed normalised difference vegetation index (NDVI)), carbon density simulated with the ecosystem models* ***h,*** *LPJ-GUESS and* ***i,*** *ORCHIDEE-MICT.* ***j,*** *Linear trends of above-ground carbon density in the ecosystem models for 1982-2015.*

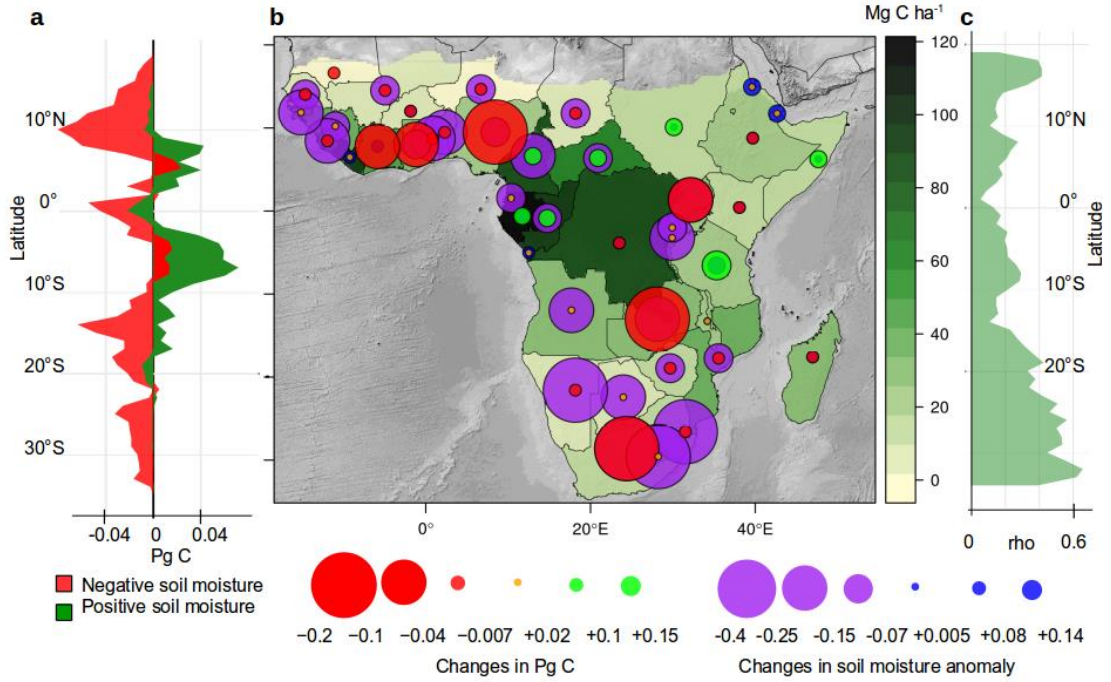

Figure 5: Soil moisture as driver of carbon stock dynamics. a, *Direction and magnitude of carbon change (2016 compared with 2010; summed per latitude) are shown for areas with positive (green) and negative (red) linear trends in soil moisture (2010-2016).* ***b,*** *Average carbon density(in Mg C ha^{-1}) and changes in carbon stocks at the country level (2016 compared with 2010) summed for each country (in Pg C). Trends in annual soil moisture (slope of linear regression for 2010-2016) averaged for each country are shown as purple (negative trend) and blue (positive trends) circles.* ***c,*** *Correlations between annual carbon stocks and annual soil moisture (Spearman's rho, n=26711) averaged along the latitudes.*

Discussion

Assessing aboveground carbon stocks and their changes using repeated inventories with a gridded sampling scheme is laborious and impossible to implement in all African countries, so assessments with short intervals for understanding changes in stocks from year to year are unrealistic at continental scale[18]. SMOS-IC L-VOD data provide a valuable alternative and the first tool for rapid monitoring of carbon stocks and their changes. Our comparison with an existing benchmark map[20] provided highly satisfactory correlations, supporting the utility of the data. The coarse spatial resolution (25

km) sets clear limits for the operational application of the L-VOD data set in relation to local scale forest monitoring, yet it is a major leap forward in assessments of C dynamics at the regional to global scale. Also, the applied benchmark map inevitably includes propagated uncertainty (Supplementary Table 1), and also the conversion adds some uncertainty to the final prediction. However, a deviation of L-VOD does not imply that the benchmark map is closer to reality, and an independent calibration of L-VOD with field survey, LIDAR and very high spatial resolution imagery for a stand-alone biomass product is a logical next step. For this study, however, the strong correlation between L-VOD and the benchmark map enabled us to provide a first application of low frequency passive microwaves to estimate temporal changes in C units at the sub-continental scale. The method applied in this study is preferable to optical remote sensing, because the L-VOD data are only controlled by the biomass of the vegetation and do not seem to saturate in forests. Moreover, although high frequency X-band VOD has been successfully applied for global biomass mapping[24], the X-VOD sensor is more sensitive to green vegetation and restricted to the upper green canopy layer when the vegetation is dense[23]. This is visible from a higher inter-annual variability in mean annual values of X-VOD (0.2±0.16 SD) than we observed in L-VOD (0.04±0.02 SD), and also intra-annual variations of monthly L-VOD data are low (mean amplitude of 0.2±0.13 SD). The advantage of L-VOD over previous methods is thus that it allows the continuous monitoring of carbon stocks, annually or even more frequently, for both forests and savannahs. Our results demonstrated the potential utility of L-VOD as a complementary data source for quantifying and monitoring carbon stocks for national reports and large-scale efforts, such as the United Nations Framework Convention on Climate Change (UNFCCC) and the Intergovernmental Panel on Climate Change (IPCC), especially for semi-arid regions with little inventory data.

Continuing deforestation and forest degradation supposedly contributed to the high cumulative C losses in humid areas. Forest degradation does not strongly reduce carbon stocks and is followed by permanent recovery, hence it needs to be explored whether this process may be concealed by saturation or whether it could be detected from L-VOD.

In spite of C losses presumably caused by deforestation, we found that carbon stocks in rainforests remained relatively stable over the period 2010-2016 and were not evidently correlated with variations in rainfall and soil moisture. On the other hand, carbon stocks outside densely forested areas were much more variable and were highly sensitive to climatic fluctuations, with two extreme events consisting of a very wet year in 2011 and a very dry one in late 2015-early 2016. Earlier studies[1,34,12] have often reported global increases in dryland carbon stocks, which has led to the general understanding that drylands may serve as carbon sinks. Our study found that dry years have reversed this trend for 2010-2016 in areas where such increases in woody vegetation (and thus carbon stocks) have occurred in the past (e.g. southern Africa and Senegal[1,34.35,36]), demonstrating that climate controls short-term variations in carbon stocks at large scales.

Previous studies of carbon dynamics in Africa were based on ecosystem models and optical satellite observations both only measuring changes in the green fraction rather than in biomass. Our observational data on dryland vegetation C stocks showed substantially higher values than simulated in the two ecosystem models, suggesting that models underestimate the crucial role of woody vegetation in savannahs as carbon sinks and sources[14,20]. The large losses of carbon from African drylands during 2010-2016 support the view that the large area of drylands and their highly variable carbon stocks make these ecosystems important in the global accounting of the carbon balance, even though mean carbon stocks are generally quite low per unit area. With such inter-annual variability, it is difficult to conclude from the 7 years of observation presented here if the observed trends reflect quasi-decadal variations or if it is a sign of longer-term dynamics. However, considerable losses were observed in 2010-2016, so we need to reassess whether, in the long term, woody vegetation in African savannas will indeed continue to be a carbon sink[37]. If dry years become more frequent[38], large-scale carbon losses may exacerbate climate change, particularly in dry areas. Our study thereby highlights the importance of timely monitoring of both tropical deforestation and the highly dynamic woody carbon stocks of savannah ecosystems for assessments of global carbon stocks.

Data and Methods

Passive microwaves for soil moisture, VOD and carbon estimation. The estimates of biomass were computed from the SMOS L-VOD product in the IC version[39]. It is a global product gridded at 25 km spatial resolution and 1-day temporal frequency. The SMOS products (soil moisture and L-VOD) are computed from a two-parameter inversion of the L-MEB model (L-band Microwave Emission of the Biosphere) from the multi-angular and dual-polarized SMOS observations[26,40]. Soil moisture and L-VOD products are independent and weakly correlated (Fig. 1c). In the newly developed IC version, these products are independent of the use of auxiliary data from other space-borne observations or simulations from atmospheric models (only surface temperature estimates from ECMWF (European Centre for Medium-Range Weather Forecasts) products are used in the L-MEB inversion). We applied several steps of filtering to retrieve relatively robust and stable annual estimates: First, water bodies and pixels with on average less than 30 valid observations per year were masked out from the analysis. Then, daily L-VOD values were aggregated to yearly (median) values for 2010-2016. If less than 50 observations were valid for a particular year, the pixel values of these years were replaced by the long-term mean. This left 82% (2010), 93% (2011), 95% (2012), 92% (2013), 93% (2014), 94% (2015) and 93% (2016) of the pixels with more than 50 observations per year which were used for the analysis. SMOS L-VOD was then converted to carbon density using the biomass map from Baccini at al.[20] (which was obtained with GLAS space-borne data and forest inventories from 2007/2008) as a reference (aggregated to 25 km by averaging) by a linear regression with mean L-VOD (2010-2016). Biomass was converted to carbon by using a factor of 0.5[20]. The coefficients from the regression were used to convert L-VOD into carbon density (Mg C ha^{-1}), which was then applied separately to each year from 2010 to 2016 to quantify the dynamics in Mg C ha^{-1}. Conversion to carbon stocks weas achieved by multiplying carbon density with the amount of hectare covered by a pixel. C stock statistics per land-cover/humidity class were derived by summing the values of the pixels.

Uncertainty. Due to the coarse spatial resolution of the SMOS data, a pixel may contain a mix of

deforestation, regeneration, livestock pressure, conservation, fires, shrub encroachment and other events, resulting in a mix of carbon gains and losses that cannot be singled out. Moreover, different land cover types (e.g. forests, cropland and savannas) are often mixed within a single pixel. The coarse spatial resolution therefore renders the clear attribution of carbon changes to specific events impossible, unless they are large scale events (like climate perturbations). Our analysis thus presents the results of large scale averages (e.g. latitudinal) and concentrates on temporal rather than spatial variations. Furthermore, although annual median values have shown to be stable, remaining noise cannot be entirely excluded, and may locally impact on inter-annual variations. It is, however, unlikely that averages per latitude, land cover class or per humidity zone are biased by noise, which is supported by the very low inter- and intra-annual variations of L-VOD (on average 0.04 and 0.2 respectively).

This study does neither aim at improving existing biomass maps nor did we assume the values of the benchmark map as free of errors and representing reality. The benchmark map includes propagated uncertainties from allometric equations, the LIDAR model and the random forest extrapolation[20]. These uncertainties are shown in Supplementary Table 1 and the numbers have to be taken into account when interpreting the results; we refer to Baccini et al.[20] for further details. Furthermore, the conversion of L-VOD to carbon density propagates uncertainty which was assessed by a 10-fold cross validation. Here the data were randomly split in 10 folds of equal size, which were used to predict the omitted values. The root of the mean squares of all folds gives the cross validated RMSE. We reported the median RMSE at the 95% confidence level for different classes as ±xy; for a full list, see Supplementary Table 1.

Yearly anomalies were calculated by the z-score: (value - mean)/standard deviation. Net C changes were estimated by the difference of the carbon maps of 2010 and 2016. Gross losses (gains) were calculated by cumulating negative (positive) differences between the consecutive years. This allows to quantify the effect of deforestation (or dry years) without considering regeneration. That calculation assigns a per-pixel deforestation fraction per pixel and per year, with a corresponding amount of C regrowth being deduced from the deforestation rate during the next year.

As for L-VOD, soil moisture from the SMOS mission[29,40] was applied in the IC version[39]. A 30-day median was averaged for each year as a robust proxy for available soil moisture in the root zone. Although soil moisture was derived from the same sensor as L-VOD, the variables are independent thanks to the multi-angular capabilities of the SMOS sensor[40] and Fig. 1c shows that the correlation between SM and L-VOD is weak.

Rainfall data. We used CHIRPS (v2) daily rainfall data[32], aggregated to SMOS resolution (average). The number of rainy days per year were counted as days with rainfall >1 mm. Yearly anomalies in rainfall and soil moisture were calculated using the z-score: (value - mean)/standard deviation.

Landcover and humidity classes. ESA's CCI L4 land cover[27] for 2015 was aggregated to 25 km (majority). We reduced the number of classes to four (open trees/shrubs, shrubland, woodland, and rainforest), sorted by potentially increasing woody cover and carbon density. We merged all classes having scattered trees and shrubs in the class open trees/shrubs, which includes croplands along all rainfall zones, open trees, sparse vegetation and grassland. Note that areas converted from forest to cropland (e.g. in West Africa, Madagascar) are thus included in this class, which thus also includes remnants of forests, i.e. cropland/forest mosaics (Supplementary Fig. 3). Moreover, due to the large pixel size, a pixel free of trees or shrubs does not exist. Shrublands potentially have a dense woody cover, but the general capacity to store C is low due to the small size of the shrubs. Woodlands include open and closed tree cover, mostly located in the sub-humid and humid zones. This included the Miombo woodlands. Rainforest are closed forest areas around the equator and at the West African coast, located in areas above 1500 mm rainfall per year.

Additional data. Commercial satellite data were available via the NextView licence from Digital-Globe Inc. and were used for illustration (Fig. 3 and Supplementary Fig. 6). The images were from

the WorldView-2 and QuickBird-2 satellites and included multispectral imagery, which were pansharpened to a spatial resolution of 50 cm[28]. GIMMS-3g NDVI was used as a proxy for vegetation greenness. We summed the bi-monthly NDVIs for each year for 1982-2016 which is widely used to estimate the annual activity of green vegetation[42]. Annual fire frequency was derived from MOD14CMH by averaging monthly values.

Ecosystem models. ORCHIDEE (ORganizing Carbon and Hydrology in Dynamic EcosystEms) is a process-based dynamic global vegetation model (DGVM) developed for simulating carbon fluxes, and water and energy fluxes in ecosystems, from site level to global scale[43]. In this study, an updated version known as ORCHIDEE-MICT (aMeliorated Interactions between Carbon and Temperature) revision 4080 was run on an African grid using the 6-hourly CRU+NCEP reconstructed climate data at $2^o \times 2^o$ spatial resolution[44]. The ESA CCI Land Cover product[27] for the year 2010 was used to produce a Plant Functional Type (PFT) map used in ORCHIDEE-MICT model, following the methodology presented by Poulter et al.[45,46]. An updated release of the historical land-use forcing dataset LUHv2h (http://luh.umd.edu/data.shtml; updated from LUHv1[47] were applied to this reference PFT map to constrain the land-cover changes of forest, natural grassland, pasture, and cropland during the period 1860-2015 using the backward method (BM3) following Peng et al.[48]. The simulation run for this study used forced vegetation distribution maps and outputs on woody carbon density (sap- & heartwood) were resampled to L-VOD resolution (bilinear).

LPJ-GUESS[49] is a dynamic vegetation model that simulates the global distribution of vegetation as well as the carbon and nitrogen cycling within vegetation and soils. It applies a set of 12 plant functional types (PFTs) with different morphological, phenological and physiological characteristics, of which 10 represent tree types and 2 represent herbaceous vegetation. For the simulation of woody aboveground biomass, LPJ-GUESS was forced with monthly gridded meteorological station data at a spatial resolution of 0.5°×0.5° from the Climatic Research Unit of the University of East Anglia

(CRU ts 3.24.01[50]), monthly model-derived estimates of nitrogen deposition[51] and annual atmospheric CO_2 concentration based on ice core data and atmospheric observations[52,53] in a simulation for the period 1901-2015. The simulation was preceded by a 500-year spinup applying the first 30 years from the climate forcing in a repeated manner. Land use was represented with a simple implementation following Ahlström et al.[34], applying historical reconstructions of land use from Hurtt et al.[47]. Annual maps of woody carbon density (sap- & heartwood) were resampled to L-VOD resolution (bilinear).

Data availability. CHIRPS rainfall data is freely available at the Climate Hazard Group (http://chg.geog.ucsb.edu/data/chirps/). SMOS-IC soil moisture and L-VOD data will be made publicly available via CATDS (Centre Aval de Traitement des Données SMOS) upon acceptance of the manuscript. Also available for public are soil moisture and L-VOD in the versions L3 and L4 at CATDS (https://www.catds.fr/). Baccini's biomass map including an uncertainty map is freely available from Global Forest Watch. Model results and the L-VOD carbon maps are available from the authors upon request.

References

1. Brandt, M. et al. Human population growth offsets climate-driven increase in woody vegetation in sub-Saharan Africa. Nature Ecology & Evolution 1, 0081 (2017).
2. Rudel, T. K. The national determinants of deforestation in sub-Saharan Africa. Phil. Trans. R. Soc. B 368, 20120405 (2013).
3. Ciais, P. et al. The carbon balance of Africa: synthesis of recent research studies. Philosophical Transactions of the Royal Society A: Mathematical, Physical and Engineering Sciences 369, 2038–2057 (2011).
4. Williams, C. A. et al. Africa and the global carbon cycle. Carbon Balance and Management 2, 3 (2007).

5. Veiga, P. R.-, Saatchi, S., Wheeler, J., Tansey, K. & Balzter, H. Methodology for Regional to Global Mapping of Aboveground Forest Biomass. in Earth Observation for Land and Emergency Monitoring (ed. Balzter, H.) 5–32 (John Wiley & Sons, Ltd, 2017). doi:10.1002/9781118793787.ch2

6. Réjou-Méchain, M. et al. Local spatial structure of forest biomass and its consequences for remote sensing of carbon stocks. Biogeosciences 11, 6827–6840 (2014).

7. Reiche, J. et al. Combining satellite data for better tropical forest monitoring. Nature Clim. Change 6, 120–122 (2016).

8. Hansen, M. C. et al. High-Resolution Global Maps of 21st-Century Forest Cover Change. Science 342, 850–853 (2013).

9. Hill, M. J. & Hanan, N. P. Ecosystem Function in Savannas: Measurement and Modeling at Landscape to Global Scales. (CRC Press, 2010).

10. Allen, C. D. et al. A global overview of drought and heat-induced tree mortality reveals emerging climate change risks for forests. Forest Ecology and Management 259, 660–684 (2010).

11. Niang I., O.C. Ruppel, M.A. Abdrabo, A. Essel, C. Lennard, J. Padgham, P. Urquhart. Africa. In: Climate Change 2014: Impacts, Adaptation, and Vulnerability. Part B: Regional Aspects. Contribution of Working Group II to the Fifth Assessment Report of the Intergovernmental Panel on Climate Change [Barros V.R., C.B. Field, D.J. Dokken, M.D. Mastrandrea, K.J. Mach, T.E. Bilir, M. Chatterjee, K.L. Ebi, Y.O. Estrada, R.C. Genova, B. Girma, E.S. Kissel, A.N. Levy, S. MacCracken, P.R. Mastrandrea, and L.L.White (eds.)]. Cambridge University Press, Cambridge, United Kingdom and New York, NY, USA, 1199-1265 (2014).

12. Poulter, B. et al. Contribution of semi-arid ecosystems to interannual variability of the global carbon cycle. Nature 509, 600–603 (2014).

13. Yue, C. et al. Abrupt seasonal transitions in land carbon uptake in 2015. Atmos. Chem. Phys. Discuss. 2017, 1–21 (2017).

14. Bastin, J.-F. et al. The extent of forest in dryland biomes. Science 356, 635–638 (2017).

15. Schnell, S., Kleinn, C. & Ståhl, G. Monitoring trees outside forests: a review. Environmental Monitoring and Assessment 187, (2015).
16. Carvalhais, N. et al. Global covariation of carbon turnover times with climate in terrestrial ecosystems. Nature 514, 213–217 (2014).
17. Mermoz, S., Le Toan, T., Villard, L., Réjou-Méchain, M. & Seifert-Granzin, J. Biomass assessment in the Cameroon savanna using ALOS PALSAR data. Remote Sensing of Environment 155, 109–119 (2014).
18. Gibbs, H. K., Brown, S., Niles, J. O. & Foley, J. A. Monitoring and estimating tropical forest carbon stocks: making REDD a reality. Environmental Research Letters 2, 045023 (2007).
19. Saatchi, S. S. et al. Benchmark map of forest carbon stocks in tropical regions across three continents. PNAS 108, 9899–9904 (2011).
20. Baccini, A. et al. Estimated carbon dioxide emissions from tropical deforestation improved by carbon-density maps. Nature Clim. Change 2, 182–185 (2012).
21. Avitabile, V. et al. An integrated pan-tropical biomass map using multiple reference datasets. Glob Change Biol 22, 1406–1420 (2016).
22. United Nations / Framework Convention on Climate Change. Adoption of the Paris Agreement, 21st Conference of the Parties, Paris: United Nations (2015).
23. Tian, F. et al. Remote sensing of vegetation dynamics in drylands: Evaluating vegetation optical depth (VOD) using AVHRR NDVI and in situ green biomass data over West African Sahel. Remote Sensing of Environment 177, 265–276 (2016).
24. Liu, Y. Y. et al. Recent reversal in loss of global terrestrial biomass. Nature Clim. Change 5, 470–474 (2015).
25. Kerr, Y. H. et al. Overview of SMOS performance in terms of global soil moisture monitoring after six years in operation. Remote Sensing of Environment 180, 40–63 (2016).
26. Wigneron, J.-P. et al. Modelling the passive microwave signature from land surfaces: A review

485 of recent results and application to the L-band SMOS & SMAP soil moisture retrieval algo-
486 rithms. Remote Sensing of Environment 192, 238–262 (2017).
487 27. Hollmann, R. et al. The ESA Climate Change Initiative: Satellite Data Records for Essential
488 Climate Variables. Bull. Amer. Meteor. Soc. 94, 1541–1552 (2013).
489 28. Brandt, M. et al. Woody Vegetation Die off and Regeneration in Response to Rainfall Varia-
490 bility in the West African Sahel. Remote Sensing 9, 39 (2017).
491 29. Houghton, R. A. & Nassikas, A. A. Global and regional fluxes of carbon from land use and
492 land cover change 1850–2015. Global Biogeochem. Cycles 31, 2016GB005546 (2017).
493 30. Liu, J. et al. Contrasting carbon cycle responses of the tropical continents to the 2015–2016
494 El Niño. Science 358, eaam5690 (2017).
495 31. Kerr, Y. H. et al. Soil moisture retrieval from space: The Soil Moisture and Ocean Salinity
496 (SMOS) mission. IEEE transactions on Geoscience and remote sensing 39, 1729–1735 (2001).
497 32. Funk, C. et al. The climate hazards infrared precipitation with stations—a new environmental
498 record for monitoring extremes. Scientific Data 2, 150066 (2015).
499 33. FAO, Global Forest resource Assessment, FAO, Rome (2016).
500 34. Ahlström, A. et al. The dominant role of semi-arid ecosystems in the trend and variability of
501 the land CO2 sink. Science 348, 895–899 (2015).
502 35. Skowno, A. L. et al. Woodland expansion in South African grassy biomes based on satellite
503 observations (1990–2013): general patterns and potential drivers. Glob Change Biol 23,
504 2358–2369 (2017).
505 36. Stevens, N., Erasmus, B. F. N., Archibald, S. & Bond, W. J. Woody encroachment over 70
506 years in South African savannahs: overgrazing, global change or extinction aftershock? Philos.
507 Trans. R. Soc. Lond., B, Biol. Sci. 371, (2016).
508 37. Mbow, C. Biogeoscience: Africa's greenhouse-gas budget is in the red. Nature 508, 192–193
509 (2014).
510 38. Ji, F., Wu, Z., Huang, J. & Chassignet, E. P. Evolution of land surface air temperature trend.

511 Nature Clim. Change 4, 462–466 (2014).
512 39. Fernandez-Moran, R. et al. SMOS-IC: An Alternative SMOS Soil Moisture and Vegetation
513 Optical Depth Product. Remote Sensing 9, 457 (2017).
514 40. Wigneron, J.-P. et al. L-band Microwave Emission of the Biosphere (L-MEB) Model: De-
515 scription and calibration against experimental data sets over crop fields. Remote Sensing of
516 Environment 107, 639–655 (2007).
517 41. Kerr, Y. H. et al. The SMOS soil moisture retrieval algorithm. IEEE Transactions on Geosci-
518 ence and Remote Sensing 50, 1384–1403 (2012).
519 42. Fensholt, R. et al. Greenness in semi-arid areas across the globe 1981–2007 — an Earth Ob-
520 serving Satellite based analysis of trends and drivers. Remote Sensing of Environment 121,
521 144–158 (2012).
522 43. Krinner, G. et al. A dynamic global vegetation model for studies of the coupled atmosphere-
523 biosphere system. Global Biogeochem. Cycles 19, GB1015 (2005).
524 44. Viovy, N.: CRU-NCEPv4, CRUNCEP dataset, available at: http: //dods.ex-
525 tra.cea.fr/data/p529viov/cruncep/readme.htm (last access: December 2013), (2013.)
526 45. Poulter, B. et al. Plant functional type mapping for earth system models. Geosci. Model Dev.
527 4, 993–1010 (2011).
528 46. Poulter, B. et al. Plant functional type classification for earth system models: results from the
529 European Space Agency's Land Cover Climate Change Initiative. Geosci. Model Dev. 8,
530 2315–2328 (2015).
531 47. Hurtt, G. C. et al. Harmonization of land-use scenarios for the period 1500–2100: 600 years
532 of global gridded annual land-use transitions, wood harvest, and resulting secondary lands.
533 Climatic Change 109, 117 (2011).
534 48. Peng, S. et al. Sensitivity of land use change emission estimates to historical land use and land
535 cover mapping. Global Biogeochem. Cycles 31, 2015GB005360 (2017).

49. Smith, B. et al. Implications of incorporating N cycling and N limitations on primary production in an individual-based dynamic vegetation model. Biogeosciences 11, 2027–2054 (2014).
50. Harris, I., Jones, P. d., Osborn, T. j. & Lister, D. h. Updated high-resolution grids of monthly climatic observations – the CRU TS3.10 Dataset. Int. J. Climatol. 34, 623–642 (2014).
51. Lamarque, J.-F. et al. Multi-model mean nitrogen and sulfur deposition from the Atmospheric Chemistry and Climate Model Intercomparison Project (ACCMIP): evaluation of historical and projected future changes. Atmospheric Chemistry and Physics 13, 7997–8018 (2013).
52. Etheridge, D. M. et al. Natural and anthropogenic changes in atmospheric CO 2 over the last 1000 years from air in Antarctic ice and firn. Journal of Geophysical Research: Atmospheres 101, 4115–4128 (1996).
53. Keeling, C. D., Whorf, T. P., Wahlen, M. & van der Plichtt, J. Interannual extremes in the rate of rise of atmospheric carbon dioxide since 1980. Nature 375, 666–670 (1995).

Acknowledgements.

This research work was funded by CNES (Centre National d'Etudes Spatiales) through the Science TOSCA (Terre Océan Surfaces Continentales et Atmosphère) program. M.B., F.T. and R.F. acknowledge the funding from the Danish Council for Independent Research (DFF) Grant ID: DFF – 6111-00258. We thank DigitalGlobe for providing commercial satellite data within the NextView license program. PC, AV and JP acknowledge funding from the European Research Council Synergy grant ERC-2013-SyG-610028 IMBALANCE-P. TT was funded by the Swedish national space board (Dnr: 95/16). PC acknowledges additional support from the ANR ICONV CLAND grant. JC has benefited from “Investissement d’Avenir” grants managed by the French Agence Nationale de la Recherche (CEBA, ref. ANR-10-LABX-25-01 and TULIP, ref. ANR-10-LABX-0041), and from TOSCA funds from the CNES.

Author Contributions.

JPW, MB, JC, FT and RF designed the study. JPW, AAY, NR, YK and AM prepared the SMOS-IC data. PC and JC prepared the ORCHIDEE data, GS prepared the LPJ-GUESS data, CT prepared the high spatial resolution satellite data. MB, FT and WZ analysed the data. The results were interpreted by JC, JPW, TT, JP, PC, LVR, KR, CM, AV and RF. MB, KR, JC, RF, JPW and PC drafted the manuscript with contributions by all authors.

Competing financial interest. The authors declare no competing financial interests.

Materials & Correspondence. Correspondence and material requests should be addressed to M.B. (mabr@ign.ku.dk) and J.P.W. (jean-pierre.wigneron@inra.fr).

Supplementary

Table 1 | Changes in carbon per land cover and humidity zone. *Carbon density, above-ground biomass carbon stocks, net and gross (cumulative gain or loss of the consecutive years) changes and area per land cover class and humidity zone (drylands=arid+semi-arid+dry-subhumid). The cross validated RMSE is shown as ±, the propagated uncertainty from the benchmark map is shown in brackets (both uncertainty values at the 95% CL). Note that open trees/shrubs include croplands and appear along all rainfall zones (Fig 1c). Woodlands are located in sub-humid and humid zones (>600 mm rainfall) and rainforests around the equator with rainfall being above 1500 mm. See also Supplementary Figs 3,4.*

		C density (Mg C ha-1)	*C stock 2010 (Pg C)*	*C stock 2016 (Pg C)*	*Net C change * (Pg C y-1)*	*Gross C gain # (Pg C y-1)*	*Gross C loss ## (Pg C y-1)*	*Area (km² *1000)*
Land cover classes	*Shrubland*	13.1 ±3.6 (2.8)	5.3±1.4 (1)	5.3±1.4 (1)	0.002	+0.35	-0.35	4 123
	Open trees/shrubs	15.8 ±2.6 (3.3)	11.2±2.3 (2.1)	10.4±2.1 (2.1)	-0.08	+0.45	-0.54	7 030
	Woodland	41.6 ±6 (12)	22.9±3.4(7)	22.9±3.4(7)	-0.004	+0.58	-0.57	5 550
	Rainforest	112 ±12 .7(22)	24.2±3 (5)	24.1±3 (5)	-0.008	+0.29	-0.30	2 214
Humidity classes	*Drylands*	10.2 ±2.4 (2)	10.3±3.2 (1.8)	9.8±3.1 (1.8)	-0.07	+0.63	-0.70	11 322
	Humid areas	56.6 ±7.5 (14)	54.9±8.1 (11)	54.6±8.0 (11)	-0.03	+1.10	-1.13	9 923
Africa		32.5 ±4.5 (7.5)	65.5±11 (13)	64.8±11(13)	-0.1	+1.74	-1.84	21 245

** defined as the difference between 2016 and 2010*

 # defined as the time integral of all carbon gains counted positively since 2010

defined as the time integral of all carbon losses counted negatively since 2010

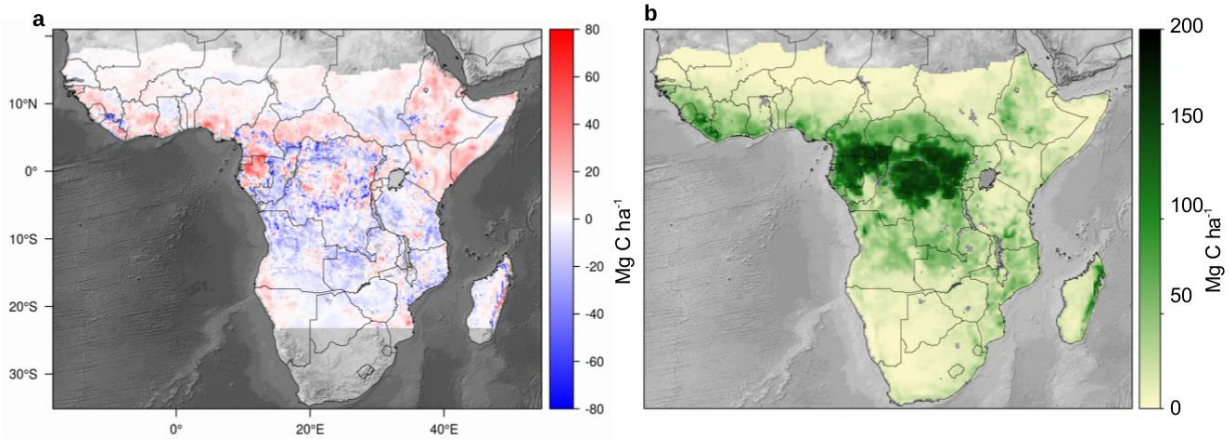

Figure 1 | a, Difference in carbon density estimated with SMOS-IC L-VOD and Baccini's benchmark map[1]. Positive (red) values mean higher values in L-VOD carbon density and negative (blue) values mean higher values in Baccini's carbon density. **b,** Carbon density estimated with SMOS-IC L-VOD (mean 2010-2016).

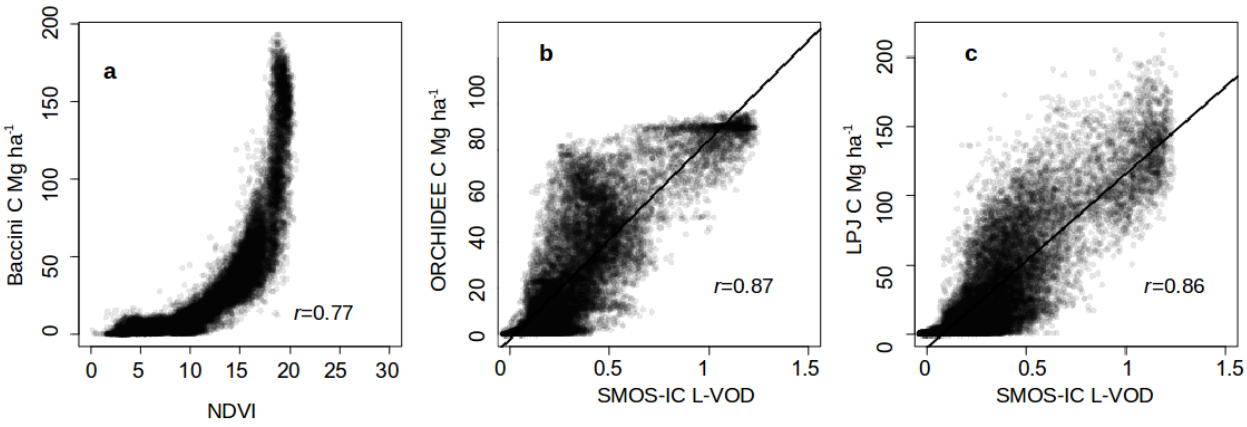

Figure 2 | Comparing **a,** optical (annually summed GIMMS-3g NDVI, mean 1982-2016). **b,** ORCHIDEE-MICT and **c,** LPJ-GUESS simulated carbon density are compared with SMOS-IC L-VOD.

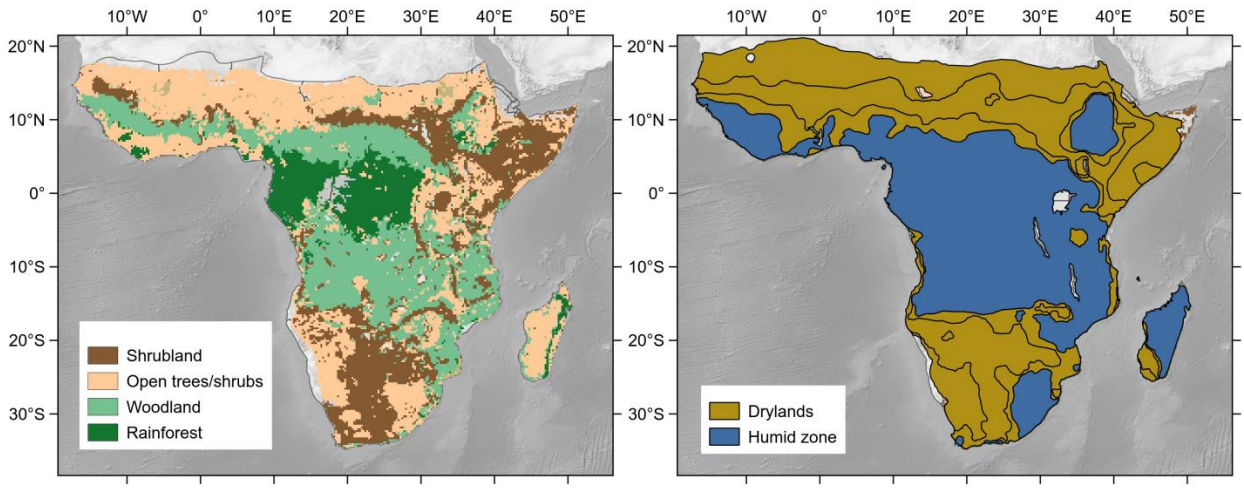

597

598

599 **Figure 3 |** ESA CCI 2015 simplified land-cover classes[3] and humidity zones. Please note that the

600 class open tree/shrub includes croplands.

601

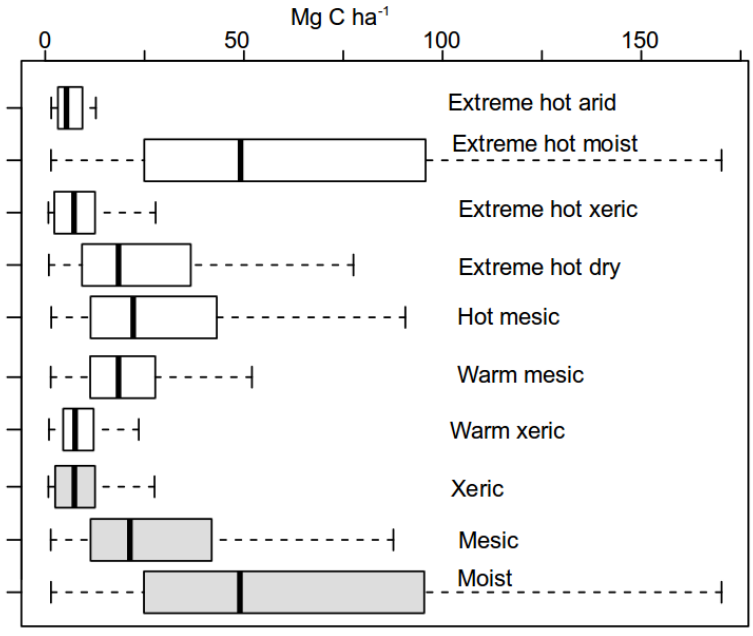

602

603 **Figure 4 |** Carbon density of the bioclimatic zones[4]. Note that the xeric, mesic, and moist zones (grey

604 bars) include the remaining sub-zones.

605

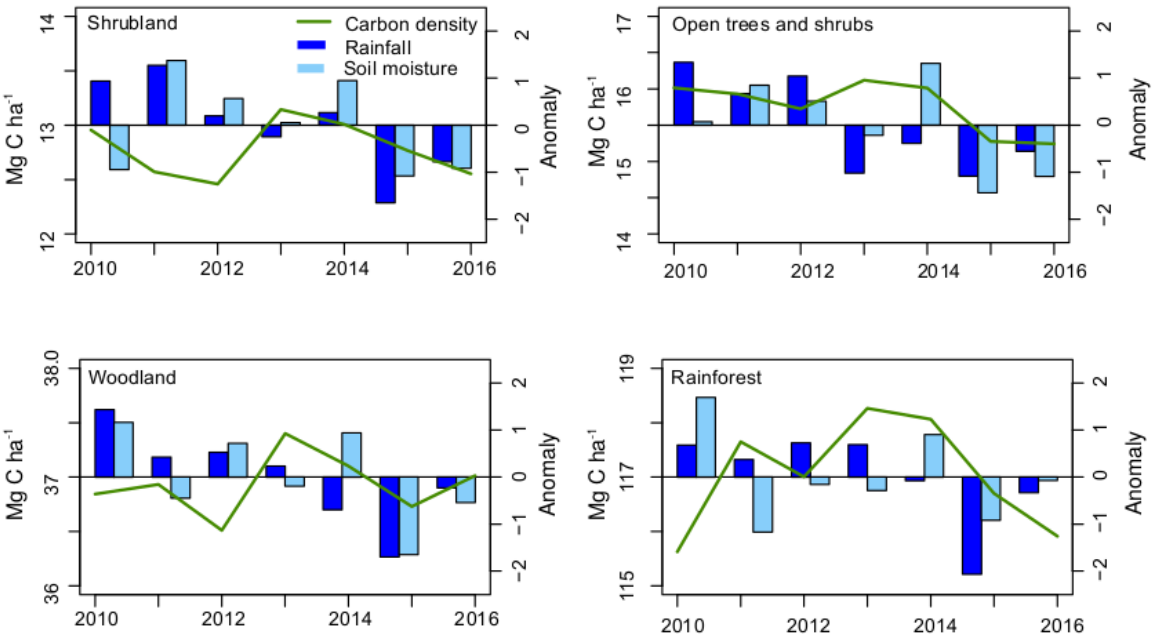

606

607

608 **Figure 5 |** Annual dynamics in L-VOD-estimated C density (in Mg C ha^{-1}), as well as rainfall and

609 soil moisture anomalies per land cover class.

610

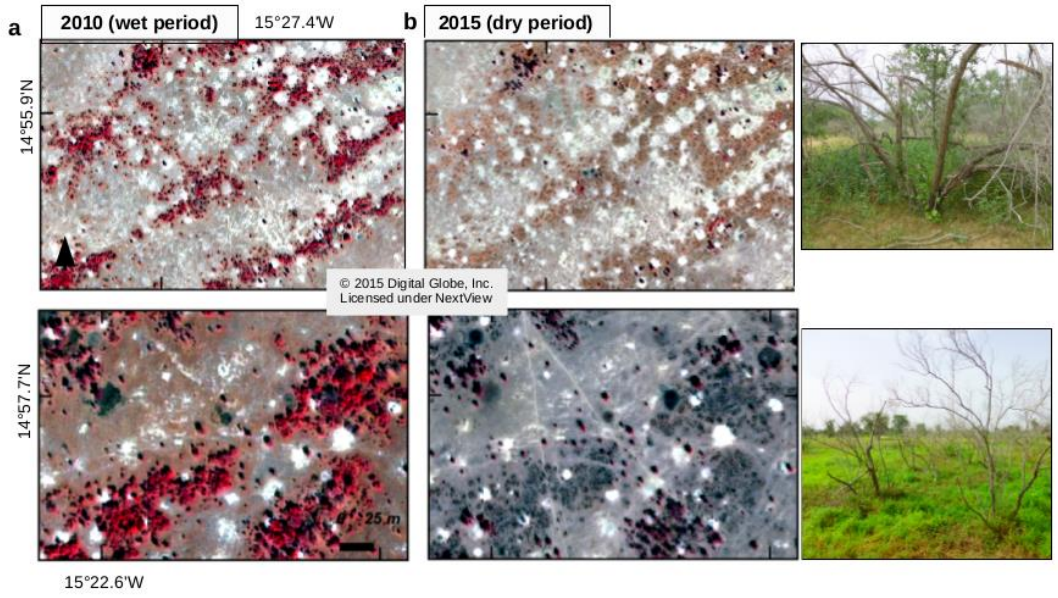

611

612 **Figure 6 |** The mass death of *Guiera senegalensis* shrubs induced by dry years in large parts of Sen-

613 egal detected by L-VOD was also documented by very high spatial resolution satellite photos and

614 field photos. The satellite images show live woody plants as red objects. **a,** The red was captured by

615 the near-infra-red channel sensing photosynthetically active leaves, which were very dense after a

wet period in 2010. Images are from late December (2010) and early February (2015), both dates where *G. senegalensis* typically has green leaves. **b,** Very limited shrub cover survived the dry period, and only large trees had photosynthesizing leaves in 2015. Photos by M. Brandt October 2015[5]. See Brandt et al.[5] for further details on the die-off.

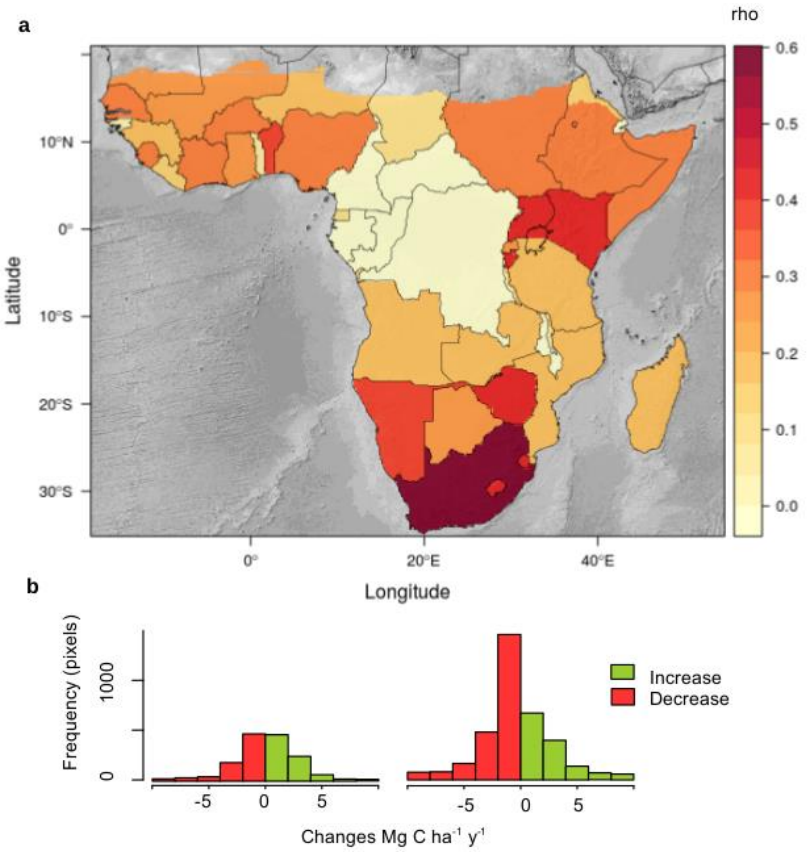

Figure 7 | a, Spearman correlation between annual C density and soil moisture, averaged per country. **b,** Left: changes in carbon density with no relationship to soil moisture (Spearman's rho <0.2). Right: changes in carbon density with a relationship to soil moisture (rho >0.2).

1. Baccini, A. et al. Estimated carbon dioxide emissions from tropical deforestation improved by carbon-density maps. Nature Clim. Change 2, 182–185 (2012).
2. Liu, Y. Y. et al. Recent reversal in loss of global terrestrial biomass. Nature Clim. Change 5, 470–474 (2015).

3. Hollmann, R. et al. The ESA Climate Change Initiative: Satellite Data Records for Essential Climate Variables. Bull. Amer. Meteor. Soc. 94, 1541–1552 (2013).

4. Olson, D. M. et al. Terrestrial Ecoregions of the World: A New Map of Life on Earth. BioScience 51, 933 (2001).

5. Brandt, M. et al. Woody Vegetation Die off and Regeneration in Response to Rainfall Variability in the West African Sahel. Remote Sensing 9, 39 (2017).